The role of seawater endocytosis in the biomineralization process in calcareous foraminifera

Shmuel Bentov[a,1,2], Colin Brownlee[b], and Jonathan Erez[a,1]

[a]Institute of Earth Sciences, The Hebrew University of Jerusalem, Jerusalem 91904, Israel; and [b]Marine Biological Association of the United Kingdom, Citadel Hill, Plymouth PL1 2PB, United Kingdom

Edited by Edward A. Boyle, Massachusetts Institute of Technology, Cambridge, MA, and approved November 2, 2009 (received for review June 14, 2009)

Foraminifera are unicellular organisms that inhabit the oceans in various ecosystems. The majority of the foraminifera precipitate calcitic shells and are among the major $CaCO_3$ producers in the oceans. They comprise an important component of the global carbon cycle and also provide valuable paleoceanographic information based on the relative abundance of stable isotopes and trace elements (proxies) in their shells. Understanding the biomineralization processes in foraminifera is important for predicting their calcification response to ocean acidification and for reliable interpretation of the paleoceanographic proxies. Most models of biomineralization invoke the involvement of membrane ion transporters (channels and pumps) in the delivery of Ca^{2+} and other ions to the calcification site. Here we show, in contrast, that in the benthic foraminiferan *Amphistegina lobifera*, (a shallow water species), transport of seawater via fluid phase endocytosis may account for most of the ions supplied to the calcification site. During their intracellular passage the seawater vacuoles undergo alkalization that elevates the CO_3^{2-} concentration and further enhances their calcifying potential. This mechanism of biomineralization may explain why many calcareous foraminifera can be good recorders of paleoceanographic conditions. It may also explain the sensitivity to ocean acidification that was observed in several planktonic and benthic species.

seawater vacuoles | biomineralization

Biomineralization is a complex biochemical process in which organisms precipitate minerals that serve for various vital functions. From a global point of view biomineralization of $CaCO_3$ in the oceans is among the major processes that control the global carbon cycle. They include the present perturbations that are associated with global change, especially atmospheric CO_2 increase and ocean acidification (1). The biomineralization process is controlled to a large extent by organic macromolecules that govern many properties of the biominerals such as crystal size and texture, crystallographic orientation, and some chemical properties of the biogenic crystals (2). Biomineralization can be intracellular (e.g., coccolithophoriids) or extracellular (most of the foraminifera and many other invertebrates, like corals and mollusks) (3). In both cases the essential ions for biomineralization require a supply system that is responsible for creating and maintaining the supersaturated conditions at the biomineralization site. Most models of calcifying invertebrates suggest that the Ca^{2+} supply to the mineralization site is based on membrane ion transporters (3–5). According to these models Ca^{2+} enters the cell passively from the extracellular medium down its electrochemical gradient through specific channels on the apical side and then actively extruded by pumps and exchangers on the basal side, which faces the calcification site.

The hyaline foraminifera are a unique experimental system for studying biomineralization on the cellular level (6). In these giant marine cells (that can be several millimeters in size) calcification is under tight biological control as can be inferred from the complex shape, structure, texture, crystallography, and chemical and isotopic compositions of their shells (1, 2). During normal calcification, foraminifera build their new calcite chambers over their previous shell. Decalcified specimens of the benthic foraminiferan *Amphistegina lobifera* when allowed to settle onto glass coverslips spontaneously precipitate new calcite shells onto the glass substrate (Fig. 1), allowing high-resolution light and confocal laser scanning microscopy (6). The new chambers are covered by secondary lamella of calcite that in this specimen is apparent as crystal aggregates forming a layer over the glass (marked as "sc" in Fig. 1). This system provides a unique model for detailed in vivo visualization of the $CaCO_3$ precipitation, including the intracellular components that are involved in this process. In this report we describe observations on the biomineralization processes of *A. lobifera* using light microscopy, fluorescent dyes, and confocal laser scanning microscopic imaging. Using these techniques we propose a pathway for biomineralization that is based on bulk seawater endocytosis as the main mechanism for the ion supply.

Results

Specimens of *A. lobifera* were partially decalcified with EDTA for several days (see *Methods*). When these specimens were transferred to normal seawater they start to recalcify their shell over the glass substrate (Fig. 1). At the beginning of the calcification process, the organism generates a sheet-like cytoplasmic structure (similar to lamellipodium), which adheres to the substrate (Fig. 2*A*). This structure is considerably different from the typical reticulated filamentous pseudopodia seen normally in foraminifera (7). The cytoplasmic sheet expands and creates a delineated microenvironment in which calcification proceeds directly onto the glass substrate. The calcite crystal units grow and form chamber walls with lobated structures, perforations, and crystallographic radial texture, which are typical for this species (Fig. 1) (6). The cytoplasmic sheet that covers the calcification site is highly vacuolated (with vacuole sizes up to 50 μm) and displays intensive organelle trafficking within well defined cytoplasmic "streams" (Fig. 2*B*). During their cytoplasmic journey, the vacuoles frequently adhere to the growing crystals for a few minutes before continuing on (Fig. 2*B*). This indicates that these vacuoles may play a role in the calcification process. To investigate the role of these vacuoles we used the fluorescent probe FITC-dextran (10 kDa) as a marker for seawater uptake via fluid phase endocytosis (Fig. 3). Labeling experiments with the dye FITC-dextran followed by incubations with normal seawater (pulse–chase) indicated that fluid phase uptake was apparent in three distinct vesicle populations, distinguished by size, pinocytotic (<1 μm), macropinocytotic (1–5 μm), and large vacuoles (>5 μm and up to several tens of

Author contributions: S.B., C.B., and J.E. designed research; S.B., C.B., and J.E. performed research; S.B., C.B., and J.E. contributed new reagents/analytic tools; S.B., C.B., and J.E. analyzed data; and S.B. and J.E. wrote the paper.

The authors declare no conflict of interest.

This article is a PNAS Direct Submission.

[1]To whom correspondence may be addressed. E-mail: bentovs@bgu.ac.il or erez@vms.huji.ac.il.

[2]Present address: Department of Biotechnology Engineering, Ben Gurion University of the Negev, Beer-Sheva 84105, Israel.

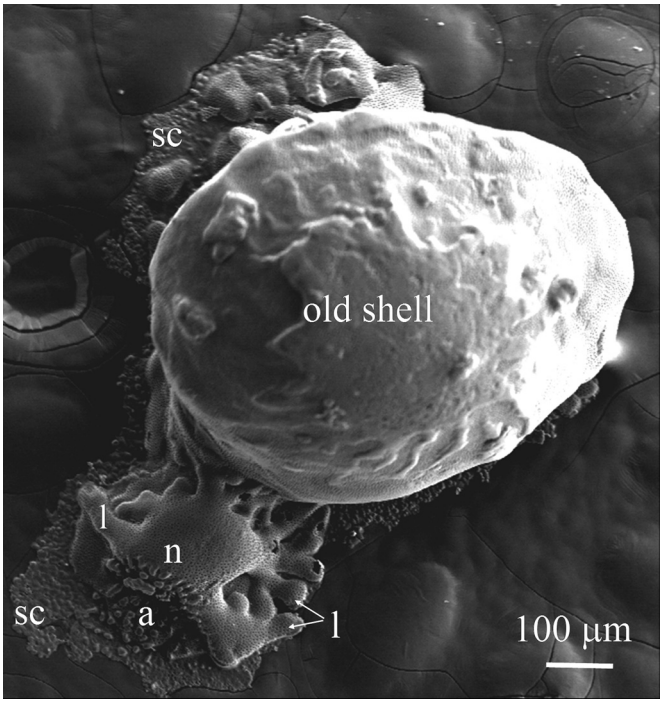

Fig. 1. SEM image of recalcified specimen of *A. lobifera*. The new chamber was built on the glass substrate instead of on the existing shell. Nevertheless, it displays all normal features of *A. lobifera* chamber. *n* = new chamber, a = aperture, l = lobes, sc = secondary crystals (consisting a layer of calcite, which is a part of the lamination process of these foraminifera).

micrometers). While the first two endocytotic pathways have been described in various eukaryotic cells (8, 9), the process of large vacuoles (SWV) formation has not been described hitherto. This process starts in the cell periphery where reticulated pseudopodia create vacuolar structures that display very intensive fusion and fission activity (Fig. 3*A*). Although the filling of the vacuoles is not instant, as in pinocytosis, it occurs relatively fast and takes 10–25 min at which time the intensity of the fluorescent signal in them equals that of the external medium. At the initial stage the vacuoles are semi open to the outer seawater probably in the form of deep membranal invaginations rather than "true" sealed vacuoles. The filling of the vacuoles may be mediated by narrow tubular channels, which appear as labeled threads in Fig. 3*A*. Similar tubular channels, which are interconvertible with large vacuoles and convey external fluids to

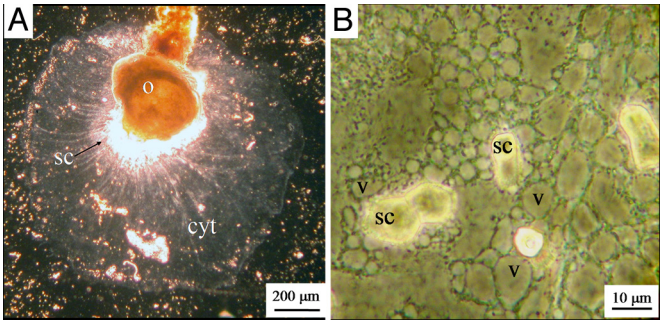

Fig. 2. The cytoplasm of a recalcifying *A. lobifera*. (*A*) The cytoplasmic layer (cyt) that delineates the calcification site. (*B*) Precipitation of secondary calcite crystals (sc) on the glass underneath the highly vacuolated cytoplasmic layer. Some of the vacuoles (v) are attached to the newly precipitated calcite aggregates.

cellular vacuoles, were documented in other amoebas (10). From the semiopen invaginations smaller vacuoles, usually in the size of few tens of micrometers, pinch off, and start to travel in the cytoplasm. Based on chase incubations, the residence time of seawater in the sealed vacuoles seems to strongly depend on the calcification process. Seawater vacuoles of calcifying specimens display a short residence time of <1 h while noncalcifying specimens, which are between chamber formation episodes, display a residence time of >48 h.

During pulse–chase experiments with FITC-dextran, we observed that the $CaCO_3$ that was precipitated during the pulse period was slightly labeled by the fluorescent dye (Fig. 4 *A* and *B*). The physical basis for the incorporation of FITC-dextran into growing calcite is not yet clear, however, it was reported previously that dextran molecules tend to be adsorbed on growing $CaCO_3$ crystals (11). The incorporation of the dye to the $CaCO_3$ during the pulse period may represent direct supply of labeled ambient seawater to the "extracellular" calcification site, not necessarily connected to the vacuolization process. However, the $CaCO_3$ that was deposited during the chase period (after the labeled medium was replaced with normal seawater), was also strongly labeled by FITC-dextran (Fig. 4 *C* and *D*). At this stage the only source for the dye is the seawater vacuoles inside the organism. This strongly indicates that the seawater-derived contents of the SWVs are brought to the active calcification site, where they may serve as the calcifying solution. Because the FITC-dextran is a membrane-impermeable dye this also indicates that the seawater transport is not mediated by transmembrane pathways. We repeated this experiment with the fluorescent dye calcein, a known membrane-impermeable calcium chelator that is readily incorporated into $CaCO_3$ during its precipitation (12). The results (Fig. 5) were similar to those obtained with FITC-dextran and showed that during the chase period, the newly deposited $CaCO_3$ was indeed strongly labeled with calcein. Because the only source for the dye is the seawater vacuoles, these observations strongly indicate a direct contact of the growing calcite with the vacuolated seawater.

The regular endocytotic processes (e.g., pinocytosis, macropinocytosis, and phagocytosis) differ in their formation and their cellular pathways and serve different functions, however, they all involve acidification of the internalized fluids to pH values of less than six (8, 9). Acidified seawater would not favor calcification (13, 14) and could induce dissolution because the concentration of CO_3^{2-} and accordingly the calcite saturation ($\Omega = [Ca^{2+}] \times [CO_3^{2-}]/K'sp$ calcite), drops dramatically with the pH. To verify the role of the large seawater vacuoles in the calcification process, their pH was evaluated with the membrane impermeable fluorescent pH probe SNARF-1dextran, which was added to the surrounding seawater (Fig. 6). Observations of vacuoles containing SNARF-1 indicate that alkalization may take place within a 30-min period, to a pH of 8.7 ($\pm$ 0.1), ~0.5 pH unit above the external seawater. The alkaline vacuoles could be clearly distinguished from the ambient seawater (pH = 8.2) and the acidic endosomes, which show low pH (<6) (Fig. 6). The pH of the cytosol, was estimated with the membrane-permeable pH probe SNARF-1-AM, to be in the range of 7.2 to 7.5, which is consistent with the reported values for other marine organisms (15, 16).

Discussion

The observations described above strongly support a major role for seawater vacuolization in the ion supply for shell calcification in *A. lobifera*. The seawater vacuoles undergo a pH increase and possibly other chemical modification (see below) and are then exocytosed into the delineated calcification site. This method would represent an efficient way for Ca^{2+} and CO_3^{2-} supply to the growing crystals. The alternative transmembrane transport of large amounts of Ca^{2+}, needed for new chamber formation,

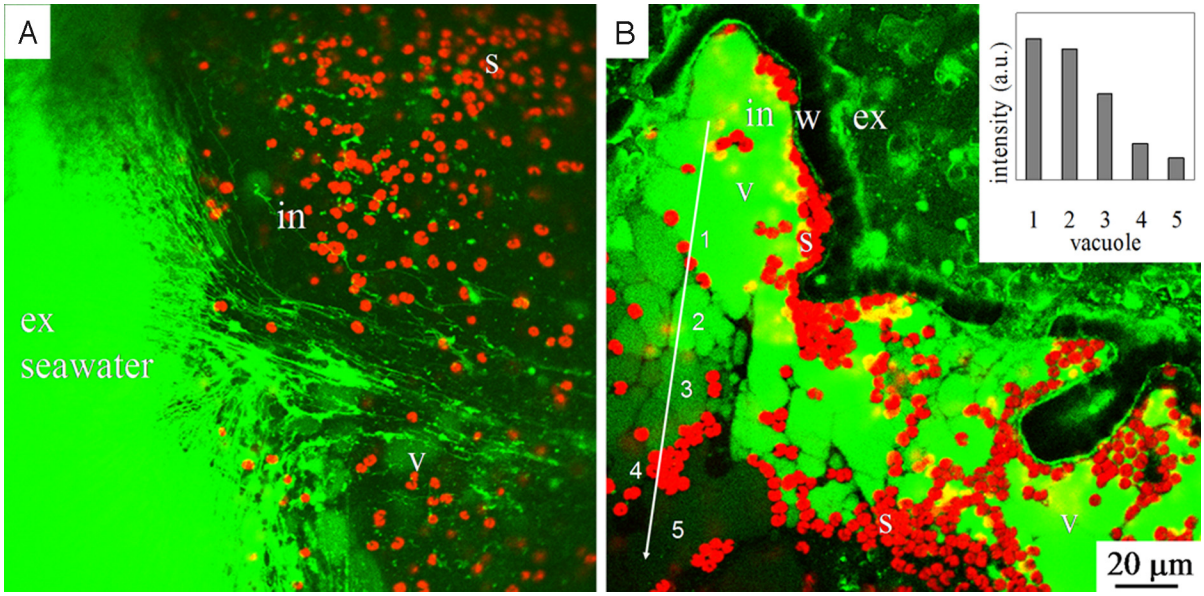

Fig. 3. FITC-dextran labeled seawater demonstrating endocytosis. (*A*) Labeled threads (green) associated with the inward cytoplasmic stream and the formation of new vacuoles (v). The symbiotic algae (s) with their red autofluorescence are intracellular (in). (*B*) Seawater vacuoles in the last peripheral chamber after 25 min of incubation. The yellow color represents combined signal of red (algae) and green (FITC in SWV) fluorescence. (*Inset*): The average fluorescence intensity of five marked vacuoles along the arrow, note the gradual inward decrease of the fluorescence. v = vacuoles, in = intracellular, ex = extracellular, w = chamber wall, s = algae symbionts.

through the cytosol is problematic because the cytosolic-free Ca^{2+} concentration is usually <1 μM (17). The massive calcium transport entails very large energy expenditure, cytotoxic dangers, and Ca^{2+} diffusion-rate limitations (18–21) especially in the extremely large cells of foraminifera. The vacuolar pathway obviously minimizes these problems. It can bring Ca^{2+}-enriched

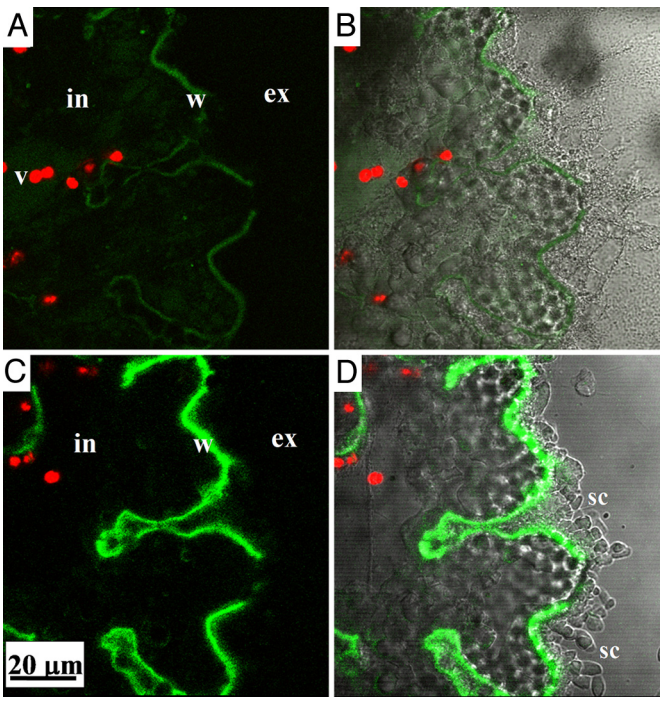

Fig. 4. Calcification from seawater vacuoles labeled with FITC-dextran: (*A*) At the end of a 2-h pulse, the labeled calcite represents calcification during the incubation period. (*B*) The same images as *A*, merged with transmitted light channel. (*C*) After 24 h of chase (in dye-free seawater) the fluorescence signal of the FITC-dextran has increased, while the only source for the dye is the intracellular seawater vacuoles. (*D*) The same images as *C*, merged with transmitted light channel. v = vacuole, in = intracellular, ex = extracellular, w = chamber wall, sc = secondary crystals.

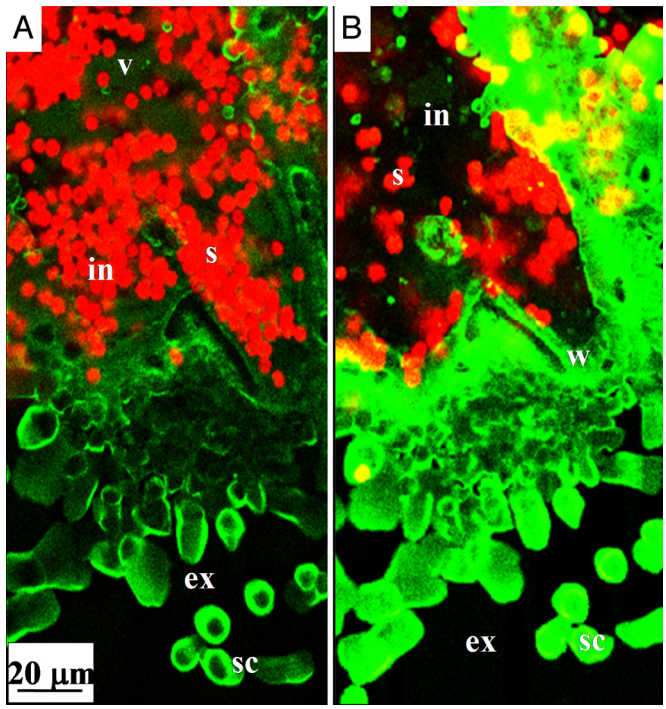

Fig. 5. Calcification from seawater vacuoles labeled with calcein: (*A*) At the end of a 1-h incubation with the dye (pulse) followed by washing with normal seawater (chase), the labeled outline of the chamber represents the calcification during the pulse incubation. (*B*) After 24 h of chase, the chamber wall is thicker, and the labeled calcite strip has expanded when the only source for the calcein is the labeled seawater vacuoles. v = vacuoles, in = intracellular, ex = extracellular, w = chamber wall, s = algae symbionts, sc = secondary crystals.

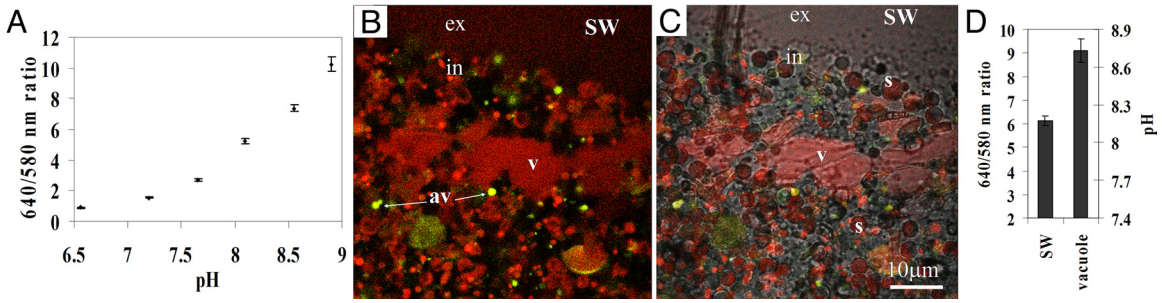

Fig. 6. pH imaging of seawater vacuoles with SNARF-1 dextran. (*A*) In vitro calibration of SNARF-1 fluorescence in seawater (error bars = STD). (*B*) Alkaline seawater vacuoles. The image composed of green and red representing the 580- and 640-nm fluorescence, respectively. (*C*) The same image merged with transmitted light channel. (*D*) The emission ratio 640/580 nm, and the corresponding pH, of the large seawater vacuole (v) and the surrounding seawater. The small vesicles with bright yellow color (av) are acidic (pH <6) as indicated by their low 640/580 fluorescence ratio. v = vacuoles, av = acidic vesicles, in = intracellular, ex = extracellular, s = algae symbionts.

solution (≈10.5 mM in the case of seawater) to the calcification site bypassing the cytosol. The large size of the SWV implies a high volume/membrane surface area ratio, which enables an efficient seawater supply compared with smaller vesicles.

The process of seawater vacuolization is different from the typical endocytosis pathway because it involves vesicle alkalization rather than acidification. The alkalization of the vacuoles suggests that the supply of CO_3^{2-} for calcification is also mediated by the SWV (Fig. 7). pH increase in the SWV will increase the CO_3^{2-} concentration in two ways. First, it increases the relative CO_3^{2-} proportion of the total inorganic carbon (C_T) in the encased seawater. A pH increase from 8.2 to 8.7 would increase the CO_3^{2-} concentration by a factor of ≈2.5 in a close (to CO_2) system and by a factor of ≈6.7 in an open system (22) (from 300 to ≈750 and 2,000 μM, respectively). Second, when such alkaline vacuoles travel in the relatively acidic cytoplasm (pH ≈7.2–7.5), the $CO_{2\,(aq)}$ present in the cytosol would diffuse down the gradient into the alkaline vacuoles thus increasing their C_T further (Fig. 7). The process of C_T increase in the vacuoles is probably enhanced due to the high density of mitochondria around the calcification site (23, 24), which provide respiratory CO_2 and the acidic endosomes (Fig. 6) that would also release $CO_{2(aq)}$ into the cytosol. These observations are in agreement with previous studies, which

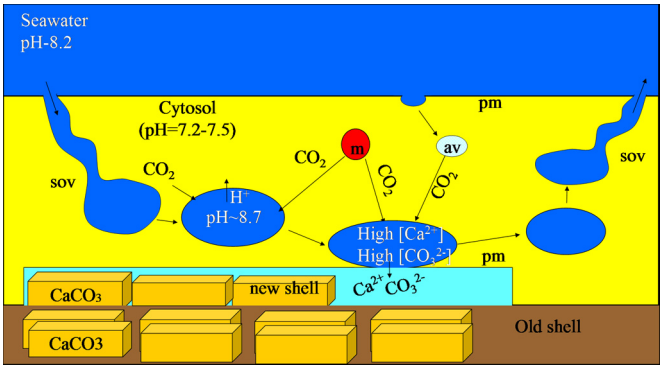

Fig. 7. Model for temporal fusion of the SWV with the plasma membrane (pm) near the active calcification site. Seawater enters the cell through deep invaginations or semi open vacuoles (sov). A vacuole is pinched off and undergoes alkalization by one of the cellular proton transport mechanisms. This SWV concentrates inorganic carbon by diffusion of $CO_{2(aq)}$ from the acidic cytosol into the alkaline SWV. This process is enhanced by adjacent mitochondria (m) and by the acidic vesicles (av) that release CO_2. The [Ca^{2+}] and [CO_3^{2-}]-enriched vacuoles fuse with the cell membrane and supply the ions for calcification. The vacuoles are then resealed and release their content apically (away from the growing crystals).

suggest that *A. lobifera* and other hyaline foraminifera have a large internal inorganic carbon (C_T) pool that is used for calcification (25). It is most likely that the C_T-enriched alkaline SWV represents this calcification-specific carbon pool. The competition for inorganic carbon between the symbionts and the host that was described in ref. 25 is also in agreement with these observations, as cytosolic $CO_{2(aq)}$ may diffuse either into SWVs or into the photosynthetic symbionts. It is also worth noting that in seawater the C_T is ≈2.1 mM, while Ca^{2+} is ≈10.5 mM. Thus, if $CaCO_3$ is precipitated from a reservoir of seawater C_T would be consumed well before the Ca^{2+}. Hence organisms that precipitate their shell directly from seawater need to concentrate C_T in the calcification microenvironment.

Recently de Nooijer et al. (26, 27) used another fluorescent pH probe (8-hydroxypyrene-1,3,6-trisulfonic acid, HPTS) to study the pH distribution in several species of foraminifera. Their observations were made on intact specimens, using a traditional fluorescence microscopy. This method may be limited by lower horizontal and vertical resolution and therefore the measured fluorescence signal possibly represents an integration of different planes, reflecting different vesicle populations. In addition the differentiation between the cytosolic and the vacuolar pH is vague because of the low resolution and the fact that HPTS is a membrane impermeable dye that does not usually label the cytosol. However, the results of de Noojir et al., obtained from intact untreated specimens, do confirm the existence of large alkaline vacuoles, as well as some acidic ones, in agreement with our observations on recalcified specimens. de Nooijer et al. also demonstrate that the phenomenon of alkaline vacuole/vesicles is general, encompassing both hyaline and miliolid species. The pH values reported by de Noojir et al. for vacuoles in the hyaline species *Cibicides lobatulus* are 8 (26) and ≥9 (27). However, as was noted by those authors, pH measurements with HPTS can be reliably reconstructed only between 6.0 and 8.5 (26), thus, the high pH values they report may fall at the edge of the reliable range. On the other hand, it is conceivable that vacuolar pH can be somewhat variable. Vacuole pH may be affected by several parameters, such as, vacuole age in the cell, calcification rate, and CO_2 availability (which introduces a buffering effect). Obviously, interspecies variability may also account for differences in vacuolar pH.

The biomineralization mechanism proposed here may explain the relative fidelity by which foraminiferal shells record the ambient seawater chemistry and its stable isotopes. It is also consistent with the model proposed by Elderfield et al. (28) to explain some of the deviations of distribution coefficients for trace elements in foraminiferal shells, suggesting that seawater is the calcifying solution. The proposed mechanism is also consistent with the reduction of foraminiferal calcification in

response to atmospheric CO_2 increase (1) and to changes in CO_2 during glacial interglacial periods (29). The initial saturation state of the encased seawater determines the amount of energy that the foraminiferan has to spend to reach the required pH and consequently to maintain the desirable calcification rate. It is noteworthy that when major calcifiers in the ocean, like foraminifera, coccolithophores and corals, lower their calcification rate, it provides a small but significant negative feedback mechanism to global CO_2 increase.

Methods

Recalcifying Preparation. *A. lobifera* were placed in seawater that was acidified to pH ≈4 by EDTA (6 mM). After 5 days, partly dissolved specimens were transferred to normal seawater where they started recalcifying on the glass substrate.

Scanning Electron Microscopy. The samples were first treated with NaOCl (5%) to oxidize the organic matter. Samples were coated with gold in a vacuum evaporation system and observed with JEOL JXA 8600.

Fluid Phase Endocytosis Imaging. The foraminifera were incubated in seawater with 50 μM FITC dextran (MW 10,000: Sigma–Aldrich) or 20 μM calcein (Sigma–Aldrich) for various periods and then washed for the chase periods. The markers were excited by a 488-nm laser band of an argon ion laser. The emission was split by the use of a 550-nm beam splitter to distinguish between the green fluorescence of FITC and Calcein, and the red autofluorescence of the symbiotic algae.

pH Imaging. We used the fluorescent pH indicator SNARF-1 (Molecular Probes) for single excitation dual-wavelength emission ratiometric measurement of pH. The advantage of ratio dyes is that, although the ratio of fluorescence intensities is pH-dependent, it is independent of dye concentration or localization (30). The emission spectrum of SNARF-1 (pK = 7.5) showed clear pH-dependent shifts, and emission ratios calculated from 640 and 580 nm are a sensitive indicator of pH (640-nm emission increases with pH while 580-nm emission decreases with pH). In vitro calibration with seawater solutions of known pHs was performed (Fig. 6*A*). During the experiment we used a real-time reference solution, namely is the surrounding seawater with its known pH. A single point calibration was performed for each experiment to standardize pH calculation. To eliminate the possibility of intracellular effect on the emission ratio, which is not pH-dependent, we compared the ratio in the external seawater with the ratio in newly formed vacuoles, before pH rise, and confirmed they show the same ratio. Vacuolar pH imaging was performed by incubation with 50 μM SNARF-1 dextran (MW 10,000 Molecular Probes), which is membrane impermeable. Cytosolic pH imaging was performed by incubation of the foraminifera in seawater with 10 μM SNARF-1-AM (Molecular Probes), which is membrane permeable. For excitation we used the 514-nm band of argon laser or 543-nm band of a He-Ne laser. The emission was split by a 610 beam splitter filter and further by narrow band filters 580 and 640 to separate the fluorescence peak of 580 and 640 for ratio calculation. To analyze ratio images, mean pixel intensity was calculated from the vacuoles and the ambient seawater for each channel (580 and 640 nm), using the ImageJ software (National Institutes of Health).

ACKNOWLEDGEMENTS. We thank Prof. M. Edelman for critically reading the manuscript and the staff at the Interuniversity Institute of Eilat for technical help and use of facilities. This work was supported by U.S.-Israel Science Foundation Grant 2000284 and German-Israeli Foundation Grant G-720-145.8/01.

1. Erez J (2003) The source of ions for biomineralization in foraminifera and their implications for paleoceanographic proxies. *Rev Mineral Geochem* 54:115–149.
2. Lowenstam HA, Weiner S (1989) *On Biomineralization* (Oxford Univ Press, Oxford).
3. Simkiss K, Wilbur K (1989) Biomineralization. Cell Biology and Mineral Deposition (Academic, Inc., San Diego).
4. Marshall AT, Clode PL (2002) Effect of increased calcium concentration in sea water on calcification and photosynthesis in the scleractinian coral *Galaxea fascicularis. J Exp Biol* 205:2107–2113.
5. Wheatly MG, Zanotto FP, Hubbard MG (2002) Calcium homeostasis in crustaceans: Subcellular Ca dynamics. *Comp Biochem Phys B* 132:163–178.
6. Bentov S, Erez J (2005) Novel observations on biomineralization processes in foraminifera and implications for Mg/Ca ratio in the shells. *Geology* 33:841–844.
7. Travis JL, Bowser SS (1986) Microtubule-dependent reticulopodial motility: Is there a role for actin? *Cell Motil Cytoskeleton* 6:146–152.
8. Swanson JA, Watts C (1995) Macropinocytosis. *Trends Cell Biol* 5:424–428.
9. Cardelli J (2001) Phagocytosis and macropinocytosis in *Dictyostelium*: Phosphoinositide-based processes, biochemically distinct. *Traffic* 2:311–320.
10. Gerisch G, Heuser J, Clarke M (2002) Tubular-vesicular transformation in the contractile vacuole system of *Dictyostelium. Cell Biol Int* 26:845–852.
11. Hardikar VV, Matijevic E (2001) Influence of ionic and nonionic dextrans on the formation of calcium hydroxide and calcium carbonate particles. *Colloids Surf A Physicochem Eng Asp* 186:23–31.
12. Bernhard JM, Blanks JK, Hintz CJ, Chandler GT (2004) Use of the fluorescent calcite marker calcein to label foraminiferal tests. *J Foraminiferal Res* 34:96–101.
13. Allemand D, et al. (2004) Biomineralisation in reef-building corals: From molecular mechanisms to environmental control. *Comptes Rendus Palevol* 3:453–467, 2004.
14. Marubini F, Ferrier-Pages C, Furla P, Allemand D (2008) Coral calcification responds to seawater acidification: A working hypothesis towards a physiological mechanism. *Coral Reefs* 27:491–499.
15. Payan P, Girard JP, Ciapa B (1983) Mechanisms regulating intracellular pH in sea-urchin eggs. *Dev Biol* 100:29–38.
16. Nimer NA, Brownlee C, Merrett MJ (1999) Extracellular carbonic anhydrase facilitates carbon dioxide availability for photosynthesis in the marine dinoflagellate *prorocentrum micans. Plant Physiol* 120:105–112.
17. Alberts B, et al. (2002) *Molecular Biology of the Cell* (Garland Science, New York), 4th Ed.
18. Anderson OR, Faber WWJ (1984) An estimation of calcium carbonate deposition rate in a planktonic foraminifer *Globigerinoides sacculifer* using ^{45}Ca as a tracer: A recommended procedure for improved accuracy. *J Foraminiferal Res* 14:303–308.
19. Bronner F (1991) Calcium transport across epithelia. *Int Rev Cytol* 131:169–212.
20. Bronner F (1990) Intestinal calcium transport: The cellular pathway. *Miner Electrolyte Metab* 16:94–100.
21. Hubbard MJ (2000) Calcium transport across the dental enamel epithelium. *Crit Rev Oral Biol M* 11:437–466.
22. Zeebe RE, Sanyal A (2002) Comparison of two potential strategies of planktonic foraminifera for house building: Mg^{2+} or H^+ removal? *Geochim Cosmochim Ac* 66:1159–1169.
23. Angell RB (1979) Calcification during chamber development in *Rosalina floridana. J Foraminiferal Res* 9:341–353.
24. Angell RB (1980) Test morphogenesis (chamber formation) in the foraminifer *Spiroloculina hyaline* schulze. *J Foraminiferal Res* 10:89–101.
25. Terkuile B, Erez J, Padan E (1989) Competition for inorganic carbon between photosynthesis and calcification in the symbiont-bearing foraminifer *Amphistegina lobifera. Mar Biol* 103:253–259.
26. de Nooijer LJ, Toyofuku T, Oguri K, Nomaki H, Kitazato H (2008) Intracellular pH distribution in foraminifera determined by the fluorescent probe HPTS. *Limnol Oceanogr Meth* 6:610–618.
27. de Nooijer LJ, Toyofuku T, Kitazato H (2009) Foraminifera promote calcification by elevating their intracellular pH. *Proc Natl Acad Sci USA* 106:15374–15378.
28. Elderfield H, Bertram CJ, Erez J (1996) Biomineralization model for the incorporation of trace elements into foraminiferal calcium carbonate. *Earth Planet Sci Lett* 142:409–423.
29. Barker S, Elderfield H (2002) Foraminiferal calcification response to glacial-interglacial changes in atmospheric CO_2. *Science* 297:833–836.
30. Bright GR, Fisher GW, Rogowska J, Taylor DL (1989) Fluorescence ratio imaging microscopy. *Methods Cell Biol* 30:157–192.